Triplet Excimer Formation in a DNA duplex with Silver Ionmediated Base Pairs

Lara Martínez-Fernández,^{1,*} Forrest R. Kohl,² Yuyuan Zhang,² Supriya Ghosh,² Andrew J. Saks,² and Bern Kohler^{2,*}

¹Departamento de Química, Facultad de Ciencias and Institute for Advanced Research in Chemical Science (IADCHEM), Universidad Autónoma de Madrid, Campus de Excelencia UAM-CSIC, Cantoblanco, 28049 Madrid, Spain.

²Department of Chemistry and Biochemistry, 100 W. 18th Ave., Columbus, Ohio 43210, USA

*Corresponding Authors: lara.martinez@uam.es, kohler.40@osu.edu

ABSTRACT: The dynamics of excited electronic states in self-assembled structures formed between silver(I) ions and cyto-sine-containing DNA strands or monomeric cytosine derivatives were investigated by time-resolved infrared (TRIR) spectroscopy and quantum mechanical calculations. The steady-state and time-resolved spectra depend sensitively on the underlying structures, which change with pH and the nucleobase and silver ion concentrations. At pH \sim 4 and low dC₂₀ strand concentration, an intramolecularly folded i-motif is observed in which protons, and not silver ions, mediate C-C base pairing. However, at the higher strand concentrations used in the TRIR measurements, dC₂₀ strands associate pairwise to yield duplex structures containing C-Ag⁺-C base pairs with a high degree of propeller twisting. UV excitation of the silver ion-mediated duplex produces a long-lived excited state, which we assign to a triplet excimer state localized on a pair of stacked cytosines. The computational results indicate that the propeller-twisted motifs induced by metal-ion binding are responsible for the enhanced intersystem crossing that populates the triplet state, and not a generic heavy atom effect. Although triplet excimer states have been discussed frequently as intermediates in the formation of cyclobutane pyrimidine dimers, we find neither computational nor experimental evidence for cytosine-cytosine photoproduct formation in the systems studied. These findings provide a rare demonstration of a long-lived triplet excited state that is formed in a significant yield in a DNA duplex, demonstrating that supramolecular structural changes induced by metal ion binding profoundly affect DNA photophysics.

1. Introduction

The study of metallo-DNAs has flourished recently because their versatility and metal-based functionality make them of great interest in bioinorganic¹ and supramolecular chemistry,² and because of their promising applications in biomedicine3-4 and environmental monitoring.5 Many metal ions bind nonspecifically to the phosphate backbone of DNA, where they can promote the collapse of DNA strands into irregular, condensed structures.6 On the other hand, metal ions such as Ag+, Cu2+, and Hg²⁺ can coordinate selectively to nucleobases and form metalmediated base pairs.4, 7-10 The highly directional bonds between the nucleobases and metal ions facilitate the formation of ordered supramolecular structures that extend the structural vocabulary of DNA.4, 10-11 In addition to structural effects, bound metal ions confer new electronic properties to DNA through metal ion-nucleobase interactions. For example, DNAzymes are of great interest for DNA-based catalysis¹²⁻¹³ and for metal ion sensing.4, 14

DNA has been used for many years as a supramolecular platform for organizing extrinsic chromophores into photoactive assemblies. While DNA can perturb the photophysics of extrinsic chromophores as in the case of fluorescent silver clusters, 11, 15-18 metal ions can also alter the photophysical properties of the DNA bases. 19 Most attention to date has been focused on the very short-lived singlet excited electronic states that form in

DNA strands,20-24 and triplet excited states in DNA remain poorly understood. Triplet excited states can initiate deleterious photoreactions on account of their long lifetimes either directly as in the triplet-mediated formation of cyclobutane pyrimidine dimers (CPD), or indirectly through the photosensitization of singlet oxygen.25-27 However, there is great uncertainty about the conditions that lead to the formation and persistence of triplet excited states. Furthermore, their involvement in photochemical damage has been difficult to confirm because the very low quantum yields of triplet excited states formed in DNA strands make them difficult to observe using time-resolved spectroscopy. Metallo-DNA assemblies are excellent model systems for exploring triplet states in DNA because of the dual role that metal ions play in determining the metallo-DNA structure and perturbing the electronic structure of the resulting assemblies through charge transfer (CT) interactions and heavy atom effects on intersystem crossing (ISC) rates.

Here, we characterize excited state populations and their evolution in supramolecular assemblies formed when silver ions bind to cytosine monomers and to the all-cytosine oligonucleotide, dC₂₀, using time-resolved vibrational spectroscopy and quantum mechanical calculations. Silver-cytosine DNA systems were chosen for this study because C-Ag⁺-C base pairs form supramolecular nanostructures that are highly stable and among the best characterized in solution.²⁸⁻³⁰ This high level of

structural characterization is a prerequisite for our use of highlevel quantum mechanical calculations to interpret excited state dynamics. In particular, we present evidence that a long-lived excited state that was reported previously 19 in a silver ion- dC_{20} assembly (Ag- dC_{20}) is an unusual triplet excimer state that forms between a pair of stacked cytosines. This state is reached via ISC from a CT excited state with a singlet multiplicity that acts as a doorway state. Instead of promoting ISC by a heavy-atom effect, silver ion binding stabilizes twisted arrangements of C-Ag+-C base pairs that favor triplet state formation. Finally, although triplet excimer states have been proposed to be important intermediates on the pathway to CPDs, 31 this reactive pathway is inhibited in the silver-cytosine assemblies investigated here.

2. RESULTS

2.1 Experimental Results. To understand the vibrational spectroscopic signatures of silver ion binding, IR absorption spectra were recorded for several cytosine compounds in the presence and absence of silver ions. Because of the propensity of silver ion to form C-Ag*-C base pairs by coordinating to the N3 atoms of two cytosine residues, the ratio of the moles of added silver ions to moles of cytosine was fixed at 0.5. Hereafter, we will refer to this ratio as β , and the samples formed by adding silver nitrate to a D₂O solution of dC₂₀, Cyd, and Cyt will be referred to as Ag-dC₂₀, Ag-Cyd, and Ag-Cyt, respectively. Deuterated water (D₂O) was used as the solvent because of its improved transparency in the double-bond stretching region for the vibrational spectroscopy that is of interest here.

The IR absorption spectrum of Cyd in D₂O solution (Figure 1a, green curve) has four strong bands at 1505 cm⁻¹, 1523 cm⁻¹, 1615 cm⁻¹, and 1652 cm⁻¹, and a weaker band at 1583 cm⁻¹. In the IR absorption spectrum of Ag-dC20 (Figure 1b), the two bands between 1500 and 1550 cm⁻¹ shift to higher frequency and decrease significantly in amplitude. A similar change is seen in the Ag-Cyt sample (Figure S1). The weak Cyd band at 1583 cm⁻¹ is absent in Ag-Cyd (Figure 1a) but shifts to 1590 cm⁻¹ and is better resolved in Ag-dC₂₀ (**Figure 1b**). The peaks at 1615 cm-1 and 1652 cm-1 in Cyd are replaced by a trio of peaks at 1641 cm⁻¹ (shoulder), 1663 cm⁻¹, and 1698 cm⁻¹ in AgdC₂₀. Adding silver nitrate to the ss-dC₂₀ solution to form the Ag-dC₂₀ sample causes the pD to decrease from 8.5 to 6.2. Adding the same concentration of silver nitrate to water produces no change in pH, indicating that there is a release of a small quantity of D+ when Ag-dC₂₀ is formed. Importantly, the IR absorption spectrum of Ag-dC₂₀ is approximately independent of the pD of the solution from 3.8 to 8.5 (Figure S2a).

To probe the secondary structures present, circular dichroism (CD) spectra of the various dC₂₀ samples were measured at different pH values. CD spectra of Ag-dC20 samples at pH 3.8 and pH 8.2 are similar (red and black curves, Figure S2b). These CD spectra agree with the CD spectrum reported previously for AgdC₂₀ in ref. 19 and differ from the CD spectrum of ss-dC₂₀ at pH 8.5 (blue curve, **Figure S2b**). Diluting the pH 3.8 Ag-dC₂₀ solution by a factor of ten and then re-adjusting the pH to 3.5 with a drop of concentrated deuterated nitric acid (DNO₃) yielded a dramatically different CD spectrum with a negative peak at 266 nm and two positive peaks at 288 nm and 223 nm (Figure S2b, green curve). Measurements made with a silver ion-sensitive electrode indicate that dilution is accompanied by a small release (~13%) of bound silver ions (Table S1). Given that the IR and CD spectra of Ag-dC₂₀ are virtually unchanged when the pD is varied between 3.8 and 8.5, all experiments on Ag-dC₂₀ solutions were performed at the former pH value, which is established naturally in the absence of added pH buffer components when 2.7 mM of silver nitrate is added to a 5.4 mM dC₂₀ solution.

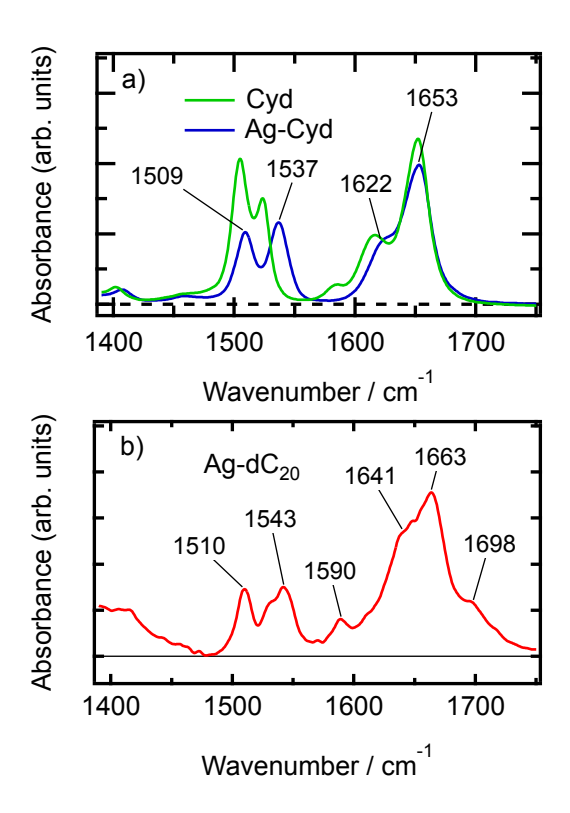


Figure 1. IR absorption spectra of a) Cyd (green) and Ag-Cyd (blue) and b) Ag-dC₂₀ (red) in D₂O. The concentration of C nucleotides is 5.4 mM for all samples. The Ag-dC₂₀ sample was made by adding 0.5 molar equivalents of AgNO₃. Frequencies in wavenumbers are shown for selected peaks in the Ag-Cyd and Ag-dC₂₀ spectra.

The excited state dynamics of Ag-dC₂₀ were studied by fs TRIR spectroscopy (**Figure 2a**). The TRIR signals were fit to the sum of three exponentials plus an offset. A global fit was performed using the same three exponential time constants for the entire dataset, while the amplitudes of each exponential term and the offset (i.e., the amplitude of an additional exponential term with a time constant equal to infinity) were optimized separately at every probe wavelength. The spectra of the amplitudes define the decay associated difference spectra (DADS) and are shown in Figure 2b next to each time constant. At delay times < 50 ps, broad positive features are seen, especially between 1400-1500 cm⁻¹ and 1560-1620 cm⁻¹, which decay with time constants of 1.0 ps and 6.7 ps (**Figure 2b**). The best-fit time constants from the TRIR measurements for Ag-dC₂₀ and the other samples are summarized in **Table 1**.

In the TRIR spectra of Ag-dC₂₀, a positive band at 1583 cm⁻¹, which is absent at the earliest delay times, grows in from 100 ps to 3600 ps (**Figure 2a**). This distinctive band is not observed in the TRIR spectra of ss-dC₂₀ (**Figure S3a**). The 1583 cm⁻¹ band rises with a time constant of 1300 ± 100 ps (**Table 1**), and this growth is reflected in the negative band at 1583 cm⁻¹ in the 1300 ps DADS (**Figure 2b**). The slow growth at 1583 cm⁻¹ is accompanied by a decrease in the amplitude of the bleach at 1667 cm⁻¹, resulting in a strong negative peak in the 1300 ps

DADS at the same frequency. The double-difference spectrum obtained by subtracting the TRIR spectrum at 150 ps from the TRIR spectrum at 3000 ps shows bands at very similar frequencies (**Figure S4**).

TRIR signals from Ag-Cyd are shown in Figure 2c and ones from Cyt and Ag-Cyt are shown in panels b and c in **Figure S3**. The Ag-Cyd signals are well described by a fitting function with two exponential terms plus an offset. The time constants were globally linked and optimized while the amplitudes were optimized separately at every probe wavelength to yield the DADS shown in **Figure 2d**. At the longest delay time (\sim 3 ns), the TRIR difference spectrum of Ag-Cyd is mostly negative between 1500 and 1700 cm⁻¹ except for a weak peak near 1580 cm⁻¹ (see the $\tau = \infty$ DADS, blue curve in **Figure 2d**). The broad, negative-going signal matches the long-time TRIR spectrum measured previously for cytosine monomers in D₂O solution without silver ions present.³² This signal is assigned to heating of the D₂O solvent due to ultrafast nonradiative decay to the electronic ground state.

To better isolate the positive feature seen near 1583 cm $^{-1}$, the signal due to hot D₂O absorption was removed from the Ag-Cyd spectrum. Unlike the Ag-dC₂₀ sample, the Ag-Cyd and Cyd TRIR

signals change minimally after 500 ps out to our longest delay time of 3400 ps. To improve the signal-to-noise ratio, the TRIR signals were averaged between 500 ps and 3400 ps to yield $\Delta A_{\rm Ag-Cyd,Avg}$ and $\Delta A_{\rm Cyd,Avg}$. The latter spectrum is assigned to hot D₂O molecules that have accepted energy due to nonradiative decay by the excited Cyd molecules. Subtracting the two averaged spectra yields the blue spectrum in **Figure 3**. Within experimental uncertainty, this spectrum compares very well with the TRIR spectrum from Ag-dC₂₀ at long delay times (red curve in **Figure 3**).

Table 1. Time Constants Obtained from Globally Fitting TRIR Signals to Sums of Two to Four Exponential Functions.^a

	$ au_1$ (ps)	τ ₂ (ps)	τ ₃ (ps)	τ ₄ (ps)
Cyt	4.00 ± 0.20	∞	-	-
ss-dC ₂₀	3.28 ± 0.10	42.2 ± 1.8	8	-
Ag-Cyt	1.39 ± 0.07	6.59 ± 0.19	8	-
Ag-Cyd	3.60 ± 0.20	39 ± 4	_∞	-
Ag-dC ₂₀	1.03 ± 0.04	6.68 ± 0.16	1300 ± 100	∞
at t		. 1 11 11		

^aUncertainties are twice the standard deviation.

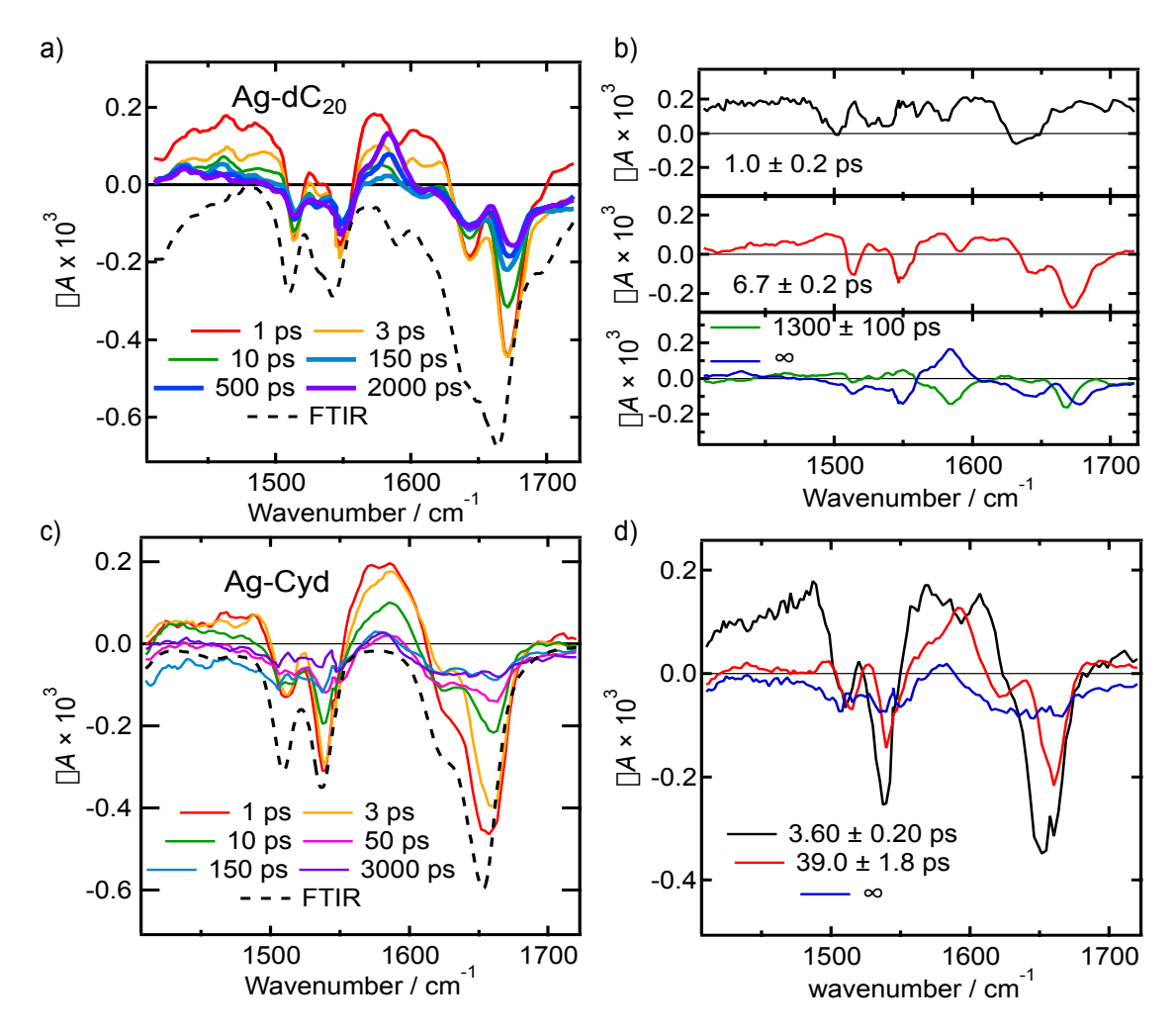


Figure 2. a) TRIR spectra of $Ag-dC_{20}$ in D_2O at selected delay times after 265 nm excitation. Spectra at times greater than 100 ps were drawn with thicker lines to emphasize the growth in the band at 1583 cm⁻¹. b) Decay associated difference spectra (DADS) of $Ag-dC_{20}$ from global fits using three exponentials plus a spectrum that is constant in time. c) TRIR spectra of Ag-Cyd at selected delay times after 265 nm

excitation. d) DADS of Ag-Cyd from global fits using two exponentials plus a time-independent spectrum. The inverted IR absorption spectrum of each sample is shown by the black dashed curves in panels a and c.

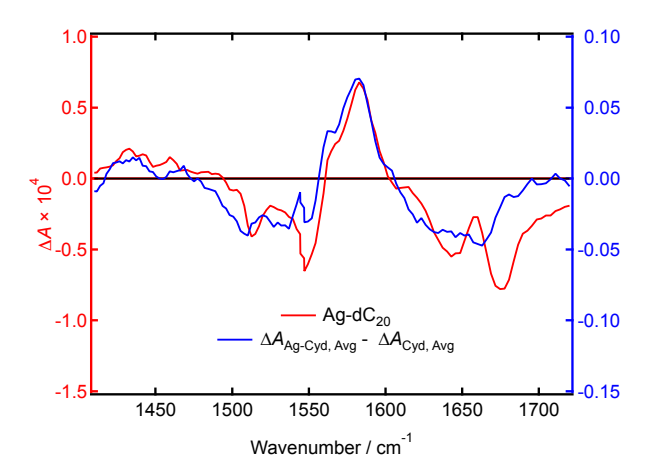


Figure 3. The transient absorption spectrum of $Ag-dC_{20}$ at 2000 ps (red curve, left vertical axis) compared with the TRIR spectrum of Ag-Cyd averaged from 500 to 3400 ps minus the TRIR spectrum of Cyd averaged over the same time range (blue, right vertical axis).

The growth of the TRIR band at 1586 cm⁻¹ for Ag-dC₂₀ is seen more clearly in the kinetic traces extracted from the TRIR dataset (red circles, **Figure 4**). At t > 100 ps, the bleach signal at 1666 cm⁻¹ (blue circles, **Figure 4**) approaches the zero-signal level (i.e., $\Delta A = 0$) in lockstep with the growth of the positive signal at 1586 cm⁻¹. In contrast, the ground state bleach (GSB) signal at 1547 cm⁻¹ (green circles, **Figure 4**) increases slightly in absolute value over the same period. The GSB signal shows that bleaching of the ground state population extends beyond our longest accessible delay time of 3.5 ns, consistent with the formation of long-lived excited states and/or photoproducts.

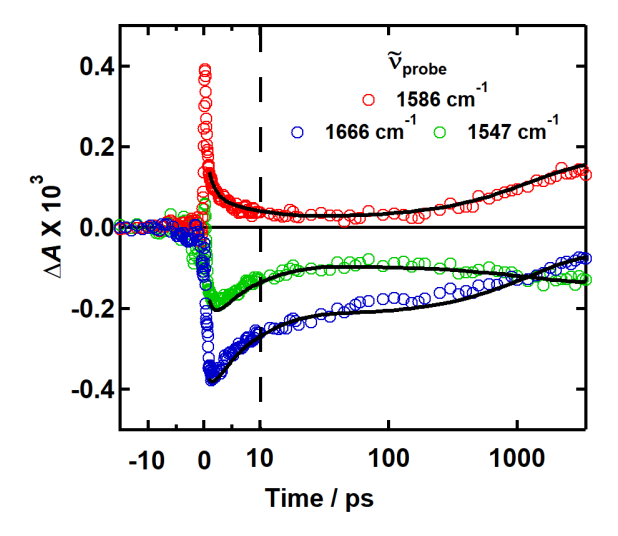


Figure 4. Kinetic traces of Ag-dC₂₀ at frequencies of 1547 cm⁻¹ (green), 1586 cm⁻¹ (red), and 1666 cm⁻¹ (blue) after 265 nm excitation. Circles are data points, and the solid black curves are

the best fits obtained from global fitting. The vertical dashed curve marks the linear-logarithmic axis break.

2.2. Computational Results. A cytosine tetramer consisting of two dC_2 strands that are joined to create two C-Ag*-C base pairs was used as the computational model for the Ag- dC_{20} experiments (**Figure 5a**). Hereafter, we will refer to this model as $Ag_2(dC_2)_2$. In each base pair, a silver ion is located approximately equidistant between the N3 atoms of each cytosine base with Ag-N3 distances of 2.2 Å. The Ag-Ag distance between the silver ions in the optimized base pairs is 3.23 Å. In each base pair, the planes of the two cytosine residues make an angle of nearly 90 deg. In contrast, the optimized ground state structure of a single C-Ag*-C base pair (**Figure 5b**), which we denote as $Ag(Cyt)_2$, lacks propeller twisting and the Cyt bases adopt a transoid, coplanar arrangement, according to the M052X/6-31G(d) level of theory.

In the optimized $Ag_2(dC_2)_2$ structure shown in **Figure 5a**, the C2-N3-N3'-C2' torsion angles are 97.6° and 94.6° in the base pairs on the 5' and 3' ends of the structure, respectively. Each base pair displays a very high value of propeller twist, which we estimated from the improper torsion angle N1-N4-N1'-N4'. Values of -74.2° and -80.0° were found for the 5' and 3' base pairs, respectively. The propeller twisting allows the carbonyl oxygen of each cytosine in the 3' base pair to accept a hydrogen bond (H bond) from the amino group of the base in the 5' base pair on the opposite strand (dashed green lines in **Figure 5a**). These interplanar H bonds (see discussion section) have short H...O distances of 1.87 – 1.89 Å.

The 10 lowest singlet excited states calculated for Ag₂(dC₂)₂ in aqueous solution at the Franck-Condon (FC) region are described in **Table S2.** To characterize excited state deactivation, all excited states below 6 eV were optimized. The minima (or conical intersections) that resulted from optimization of each vertical excited state are listed in Table S2 and the most important minima are illustrated schematically in Figure 6a. Several competing excited state decay pathways are suggested by the calculated potential energy landscape: (i) Direct decay to the ground state through a S₁/S₀ conical intersection where both upper and lower bases have bonding character (Clexc), (ii) relaxation to a minimum in the second excited state (S2), denoted $S_{\pi\pi^*}$ that is characterized by the density of a $\pi\pi^*$ state of a cytosine monomer, but which is delocalized over the two stacked bases, and (iii) decay of the $S_{\pi\pi^*}$ state to an S_1 minimum by overcoming a small barrier. At this minimum, which we designate S_{exc}, the excitation is delocalized over the two cytosines on the same strand and has bonding character between them. (iv) Alternatively, the $S_{\pi\pi^*}$ can decay to another S_1 minimum with significant CT character (S_{CT} in Figure 6a) between a single cytosine and Ag+, where 40% of the photoexcited electron moves from Ag+ to cytosine. A barrier with a height of ~0.2 eV is found along the decay pathway from the $S_{\pi\pi^*}$ state to the S_{CT} state when dynamic solvation effects are included in the calculations (see supplementary discussion in the SI). Pathways (ii) – (iv) are illustrated in Figure 6a.

Calculations were performed to locate low-lying triplet excited states of $Ag_2(dC_2)_2.$ At the S_{CT} minimum, a triplet state with $\pi\pi^*$ character ($T_{\pi\pi^*}$ in **Figure 6a**) lies very close in energy and the Spin Orbit Coupling (SOC) terms between these two states is 110 cm $^{-1}$, implying a high ISC rate. 33 For comparison, the SOC computed at the S_{exc} (<40 cm $^{-1}$) or $S_{\pi\pi^*}$ (<20 cm $^{-1}$) minima is one order of magnitude smaller. Triplet optimization from the $T_{\pi\pi^*}$ state leads to the most stable triplet minimum. This minimum has increased electron density in the π orbital region between two of the stacked cytosine units, indicative of an excimer state (T_{exc}). The C6-C6 distance between the stacked cytosines in the T_{exc} state is 2.5 Å, revealing the formation of a new bond as is observed in some excimers. $^{34-35}$

We explored the possibility of forming a cytosine-cytosine CPD from the S_{exc} and T_{exc} minima (**Figures S5 and S6**) because CPD formation should be favored in both cases by the close approach of the C6 atoms together with a decrease of the C5-C5' distance. Passage from the T_{exc} state of Ag-dC₂₀ requires overcoming a barrier of ~0.1 eV to access the T_{exc}/S_0 funnel (**Figure S6**). However, all relaxed scans from that region made by changing either the C5-C5' distance or C6-C6' distance were non-reactive. The consequences and reasons behind this different photoreactivity are explained in detail in the Discussion section (see also the Supporting Information). From the singlet manifold, the corresponding S_{exc}/S_0 CI is reached by a barrierless pathway that provides access to a stable CPD, which is located only 0.7 eV above the global S_0 minimum (Figure **S5**).

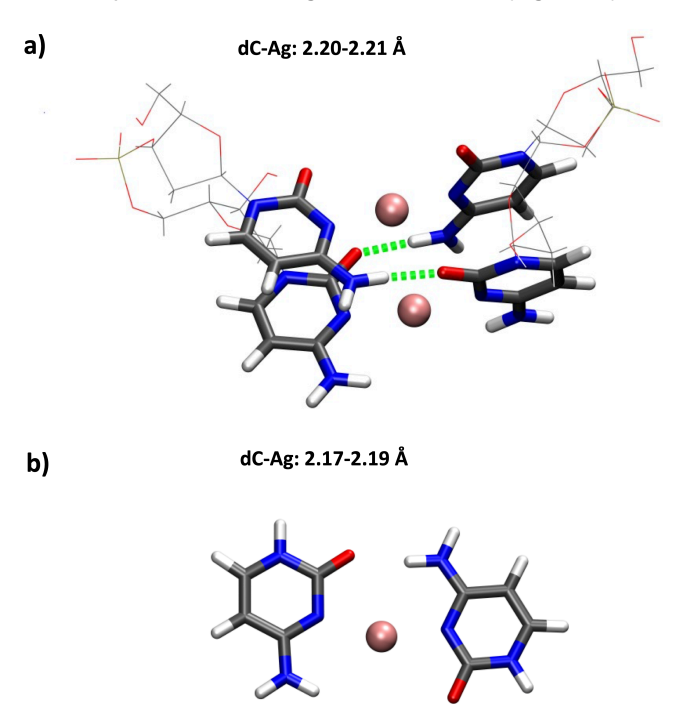


Figure 5. Computational models for a) $Ag_2(dC_2)_2$ and b) $Ag(Cyt)_2$. The QM part is depicted as sticks (nucleobase) and balls (Ag^+) whereas the MM part, the ribose phosphate backbone, is shown as a wireframe. Hydrogen bonds are depicted as

green lines. dC-Ag refers to the distance between the N3 atom and the nearest Ag ion.

Vibrational spectra of the various excited state minima were calculated to facilitate the interpretation of the TRIR measurements. Difference spectra were computed by subtracting the predicted ground state vibrational spectrum from the excited-state ones are shown in **Figure 7**.

We also modeled the excited states of a single C-Ag*-C base pair in water, Ag(Cyt)₂. The optimized structure is illustrated in **Figure 5b** and important minima are shown in **Figure 6b**. See **Table S3** for the 10 lowest singlet excited states at the ground state geometry. The calculations suggest that the FC states relax to the ground state through a conical intersection due to the same out of plane C5-C6 deformation described for cytidine. Optimization from the FC also led to the $S_{\pi\pi^*}$ and $S_{n_0\pi^*}$ minima; however the $S_{\pi\pi^*}$ minimum was found to have imaginary frequencies, indicating that it is not a true minimum. Additionally, the $S_{n_0\pi^*}$ state has a small amount of CT character with the silver ion contributing electron density to a bound cytosine. Calculated vibrational spectra for this minimum are shown in **Figure S7**, panels b and d.

3. DISCUSSION

3.1. Structural Impacts of Ag+ Binding. The CD spectra in **Figure S2b** are very similar to spectra reported in an earlier transient electronic spectroscopy study¹⁹ of the same compounds despite the threefold higher nucleobase concentrations used here. Higher concentrations are necessary for TRIR vs. transient electronic spectroscopy because vibrational absorption cross sections are much weaker than electronic ones. The similar steady-state spectra measured here and in ref. ¹⁹ suggest that common supramolecular structures are present for the millimolar nucleobase concentrations used in both studies.

Larger concentration changes induce structural changes as demonstrated by the finding that 10-fold dilution of a pD 3.8, Ag-dC20 solution followed by adjusting the pD to 3.5 yields a very different CD spectrum (Figure S2b, green curve). This CD spectrum agrees well with the CD spectrum of i-motif DNA, a structure composed of proton-mediated C-C base pairs (i.e., C-H+-C in H₂O or C-D+-C in D₂O solution).³⁷⁻³⁸ i-motif structures form when one, two, or four separate strands associate to form properly oriented C-H+-C base pairs. We propose that the low strand concentration of the dilute Ag-dC₂₀ D₂O solution favors the formation of an intramolecularly folded i-motif structure composed of C-D+-C base pairs. The concentration of deuterons slightly exceeds the silver ion concentration under these conditions ([D+] = $10^{-3.5}$ = 0.32 mM, [Ag+] = 0.27 mM), possibly favoring the i-motif structure. The observation that Ag-dC20 exhibits i-motif structure in the presence of silver ions at low strand concentration, but a parallel-stranded Ag-mediated duplex at high strand concentration reinforces the conclusion that silver ions cannot template an i-motif-like structure by taking the place of protons or deuterons. 10, 19

The dilution-induced refolding that converts C-Ag*-C base pairs to C-H*-C base pairs should be accompanied by a significant release of silver ions, but our silver ion electrode measurements indicate that 87% of silver ions remain bound after dilution of the more concentrated β = 0.5 solution (**Table S1**). This indicates that the released silver ions rebind to different sites.

Precisely where the silver ions bind is uncertain, but alternative binding sites could include amino group nitrogen atoms or backbone phosphate ions. Evidence for multiple binding sites comes from the observation that >99% of all Ag+ ions remain bound for a dC20 sample that is 2 mM in Cyt residues when $\beta=$

1.5 (see Fig. 2d in ref. 19). In this case, the 3:2 stoichiometry of bound silver ions to cytosine residues cannot be achieved by forming only C-Ag $^+$ -C base pairs.

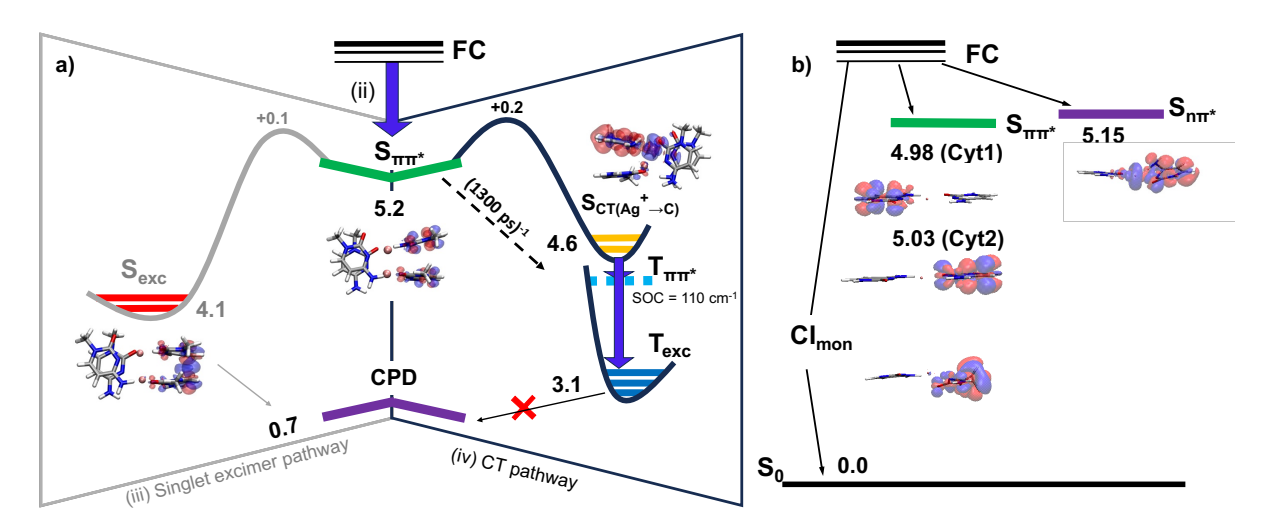


Figure 6. Calculated potential energy landscape showing excited state minima (horizontal colored lines, energies in eV are relative to the electronic ground state) for a) $Ag_2(dC_2)_2$ and b) $Ag(Cyt)_2$ in water. Energetic barriers between a few states are shown. The excited state difference density is shown for each minimum (decreased electron density is indicated by blue; increased electron density is indicated by red). Singlet and triplet (S_{exc} and T_{exc}) excimer densities are comparable. The dashed arrow in panel a illustrates the kinetic scheme used to calculate the SADS for $Ag-dC_{20}$. Wide blue arrows indicate fast kinetic steps that are not resolved.

The higher strand concentration used in all of the Ag-dC₂₀ TRIR measurements reported here, corresponding to 5.4 mM in C residues, favors the parallel-stranded dC20 duplex structure composed of C-Ag+-C base pairs.19 The CD spectra recorded for Ag-dC₂₀ at pD 3.8 and 8.2 agree well (Figure S2b), pointing to metal- and not proton-mediated base pairing at both pD values for this higher strand concentration. The pD of 6.2 that is established by adding 2.7 mM of Ag+ ions to 5.4 mM dC₂₀ (nucleotide concentration) corresponds to a very minor release of D+. Characterizing this is beyond the scope of this study, but it could reflect the loss of an amino group deuteron (possibly because it binds a second silver ion) in the terminal base pair of each duplex. Metal ion binding at N3 of cytidine is known to increase the acidity of the exocyclic amino group, and examples are known in which metal ions bind simultaneously to N3 and N4 of cytosine.³⁹ Altogether, these results reveal that the supramolecular structures induced by silver ion binding to dC₂₀ strands depend on pD, strand concentration, and Ag+ concentration and that care is needed to correctly identify the supramolecular structures actually present in solution.

We discuss next the structural insights provided by steadystate vibrational spectroscopy. Our calculations for the cytosine models with and without silver ions show strong mixing among the in-plane stretching modes in the double bond stretching region. Despite this complexity, some trends emerge. Cyt, Cyd, and dC₂₀ each exhibit a pair of bands between 1500 cm⁻¹ and 1550 cm⁻¹ (Figures 1 and S1) that are dominated by ring in-plane stretching.40-41 Both bands decrease in intensity, blue shift upon silver ion binding, and are nearly identical in appearance in Ag-Cvt, Ag-Cvd, and Ag-dC₂₀ (**Figure** 1). The silver ion-induced changes closely match ones seen when Cyd undergoes protonation (see Figure S3 in ref. 42 for the acid-induced changes in the IR absorption spectrum of 2'deoxycytidine in D₂O). Protonation of Cyt in acidic aqueous solution occurs at N3,43 the same atom that is the preferred site of silver ion coordination. Similar changes are seen for C-H+-C base pairs in parallel-stranded duplexes 44 and in i-motif DNA. 45 For both C-Ag*-C and C-H*-C base pairs, the decreased intensity of the in-plane stretching bands between 1500 and 1550 cm $^{-1}$ is likely due to depletion of π electron density in the ring. 46

We propose that the bands between 1500 and 1550 cm $^{-1}$ are highly diagnostic of C-Ag $^{+}$ -C (or C-H $^{+}$ -C) base pair formation, but relatively insensitive to secondary structure (i.e., how the C-Ag $^{+}$ -C base pairs are arranged in space). In contrast, the more intense vibrational bands seen above 1600 cm $^{-1}$ in the IR spectra of Cyt, Cyd, and dC $_{20}$ respond differently to silver ion binding. These bands, which have substantial carbonyl stretching character, are sensitive to hydrogen bonding and to the electrostatic environment. For example, these bands in Ag-dC $_{20}$ are shifted to higher frequency than the corresponding bands in Ag-Cyd (**Figure 1**) and Ag-Cyt (**Figure S1**). The different patterns of bands seen for Ag-Cyt, Ag-Cyd, and Ag-dC $_{20}$ thus provide evidence of distinct supramolecular structures.

In Ag-dC₂₀, a parallel-stranded duplex forms that is stabilized by silver ion-mediated base pairing and H bonds that link the cytosines in both strands.19,47-48 Although the silver ion can coordinate to the N3 and N3' atoms of two cytosine residues, much like an excess proton in a C-H+-C base pair, the silver ion is too large to allow two H bonds to form as is the case in each C-H+-C base pair in i-motif DNA. Calculations confirm that a single transoid C-Ag+-C base pair can form only a single H bond in its optimized geometry in which both cytosines are coplanar.⁴⁹ It is nevertheless possible to form a double-helical structure built from C-Ag+-C base pairs having a large propeller twist angle. Unlike B-DNA, where interbase H bonds always involve bases in the same base pair, each cytosine in a non-terminal C-Ag+-C base pair forms two H bonds with cytosines in base pairs above and below it. These so-called interplanar base pairs were first described in ref. ⁴⁸ and are a hallmark of parallel-stranded duplex formation in Ag-dC_n. High propeller twisting provides the high enthalpic stabilization offered by silver ion coordination while allowing each base in a non-terminal C-Ag*-C base pair to make 2 H bonds with other cytosines. The Ag-Ag distance of 3.23 Å calculated for Ag2(dC2)2 is moreover close to the rise of 3.4 Å observed in B-form DNA. Consequently, double helical structures have been detected in a variety of crystals formed when AgNO3 combines with various cytosine derivatives in a 1:2 stoichiometric ratio. $^{50-52}$

For the high Cyd concentration of 20.1 mM used in our study, the CD spectrum of Ag-Cyd differs from that of uncomplexed Cyd (**Figure S8a**). In contrast, Goncharova reported that adding silver ion does not change the CD spectrum of a dilute (60 μ M) solution of Cyd.⁵³ The CD difference spectrum computed between the CD spectrum of Ag-Cyd and bare Cyd reveals a weak component that is similar to the CD spectrum of Ag-dC₂₀ (**Figure S8b**). This suggests that the concentrated Ag-Cyd solution contains a small concentration of self-assembled structures that resemble the more abundant chiral structures present in the Ag-dC₂₀ solution. We revisit this point below in our discussion of the Ag-Cyd TRIR signals.

3.2 Photophysical Impacts of Ag+ Binding. Striking differences are seen in the TRIR spectra and dynamics of Ag-dC20, Ag-Cyd, and Ag-Cyt. These differences are attributed to secondary structure differences because the IR absorption spectra are nearly identical between 1500 cm⁻¹ and 1550 cm⁻¹, indicating that all three contain C-Ag+-C base pairs. The TRIR signals for Ag-dC20 are fit well by the sum of four exponentials, one of which is fixed to have a time constant equal to ∞, representing a signal that does not change during our probe window of 0 to 3.5 ns. Such signals typically arise in femtosecond transient absorption experiments from long-lived triplet excited states or photoproducts. For Ag-Cyd and Ag-Cyt, no persistent signal is observed beyond a weak and broad difference spectrum that is assigned to heating of the D₂O solvent.⁵⁴ In both, the excitations decay by ultrafast internal conversion to the ground state consistent with calculations on the Ag(Cyt)2 model showing only monomer-like decay. We thus focus in this section on understanding the long-lived state in Ag-dC₂₀.

We first considered whether the 1583 cm⁻¹ TRIR band arises from a $^1n\pi^*$ excited state given its proximity to the well-documented band assigned to this state at ~ 1574 cm⁻¹, which is seen in metal-free (2'-deoxy)ribose-substituted cytosine derivatives.³², ⁴⁶, ⁵⁵ Consistent with the expectation that silver ion binding will destabilize $^1n\pi^*$ excited states, our calculations for Ag(Cyt)₂ (**Table S3**) indicate that the lowest energy $^1n\pi^*$ state has excitation localized on the oxygen atom ($no\pi^*$) and is the seventh excited singlet state (S₇). Such a high-lying singlet excited state cannot have the >3 ns lifetime seen experimentally. No excited minimum with $^1n_N\pi^*$ character was located within the lowest 10 singlet excited states.

The long-lived signal contribution from Ag-dC₂₀ is doubly distinctive because of its long lifetime and slow appearance time. The unusual kinetics facilitate its assignment. Because the longest time constants of 1300 ps and ∞ are well separated from the two shortest ones, the DADS with the two longest lifetimes completely determine the dynamics after \sim 50 ps. The DADS describe how the signals change in time, but each DADS may contain contributions from two or more populations. A kinetic

mechanism is needed to calculate species-associated difference spectra (SADS) from linear combinations of the DADS.

The potential energy landscape of $Ag\text{-}dC_{20}$ that emerges from our calculations (**Figure 6a**) was used to construct a plausible kinetic mechanism. We eliminated S_{exc} (see the pathway framed in gray in Figure 6a) as the long-lived excited state because barrierless pathways lead from this state to a S_{exc}/S_0 CI (**Figure S5**). Passage through this CI, leading either back to the ground state or to the CPD photoproduct, would happen on an ultrafast timescale that is incompatible with the slow 1300 ps dynamics seen experimentally. Additionally, a persistent CPD photoproduct would indicate degradation of the $Ag\text{-}dC_{20}$ sample, but minimal degradation was observed in UV-vis and IR spectra recorded before and after laser measurements. As will be discussed in the next section, it was shown previously that silver ion binding to poly(rC) does not enhance CPD formation. 56

We used the simplified kinetic scheme shown by arrows in the pathway framed in black in Figure 6a to model the SADS of the $S_{\pi\pi^*}$ and T_{exc} states, which we propose are the only excited states that have non-negligible populations at t > 50 ps. In this mechanism, rate-limiting passage to the S_{CT} state is followed by rapid intersystem crossing to the triplet manifold and decay to the T_{exc} state. In this case, the SADS of the T_{exc} state (**Figure 7b**) is given by the DADS of the $\tau = \infty$ component. The kinetic precursor state to the T_{exc} state is the $S_{\pi\pi^*}$ state, so its SADS (**Figure 7a**) is given by the sum of the DADS with the two longest time constants.

There is no unique set of SADS as many kinetic schemes will be compatible with the number of observed decay components.⁵⁷ However, good agreement between the SADS in Figure 7 and the QM calculated difference IR spectra of excited states of the Ag₂(dC₂)₂ model duplex (**Figure 7**, right column) supports our assignments. In particular, the experimental spectrum of the long-lived state compares very favorably with the calculated TRIR difference spectrum of the T_{exc} state (**Figure 7b**). Just as in the ground electronic state, vibrational modes in the Texc state are strongly mixed, but the strong positive band in the calculated spectrum near 1600 cm⁻¹ has a strong contribution from C=C stretching. This mode down shifts from 1620 cm⁻¹ in S_0 to 1580 cm⁻¹ in T_{exc} because C5-C5' and C6-C6' bond formation in the excimer causes the C5=C6 bond to lengthen. The calculated spectrum of the localized $S_{\pi\pi^*}$ state (**Figure 7a**) agrees well with the transient spectrum seen at 150 ps (Figure **2a**). This state may contain some S_{CT} character that suppresses emission from this long-lived $1\pi\pi^*$ state. Additional calculated IR difference spectra are shown in Figure S7.

Compared to the monomers in water, very stable minima are found for the ${}^1\pi\pi^*$ states of $Ag_2(dC_2)_2$ (**Figure 6a**). This stabilization is the result of silver ion binding and increased excited state delocalization. The stabilization of the ${}^1\pi\pi^*$ state in $Ag_2(dC_2)_2$ inhibits its decay long enough to allow the excited state population to overcome the barrier to the S_{CT} state. Accounting for dynamic solvation reduces the barrier from the value of ~ 0.5 eV calculated without these effects to roughly half this value (see the Supporting Information). According to the Eyring-Polanyi equation, a barrier height of 0.25 eV predicts a

rate of $(3.2 \text{ ns})^{-1}$, which is within a factor of 3 of the observed decay rate of $(1.3 \text{ ns})^{-1}$.

The TRIR difference spectra calculated for the S_{CT} and $S_{\pi\pi^*}$ were compared with the SADS shown in **Figure 7a** to assign the precursor of the T_{exc} state. The calculated spectral signature of the S_{CT} state agrees poorly with experiment (**Figure S9**). Instead, there is good agreement with the calculated TRIR spectrum of the $S_{\pi\pi^*}$ state (**Figure 7a**). Although the S_{CT} state occurs along the path from the $S_{\pi\pi^*}$ state to the T_{exc} state, it is not detected due to its short lifetime. The S_{CT} state is nearly degenerate with a $T_{\pi\pi^*}$ state (dashed blue line in **Figure 6a**) and the spin-orbit coupling between these states is greater than 100 cm⁻¹. In this case, ISC very efficiently transfers the S_{CT} state population to the $T_{\pi\pi^*}$ state, which then rapidly decays by internal conversion to the T_{exc} state. This prevents a build-up of S_{CT} population to levels that can be detected in the TRIR experiment. Although the calculations for $Ag_2(dC_2)_2$ suggest that overcoming a low

barrier of ${\sim}0.1$ eV would allow the $S_{\pi\pi^*}$ state to relax to the S_{exc} state, the experimental evidence for a long-lived precursor state to the triplet excimer state makes this unlikely, and we propose that the singlet excimer state is populated primarily from the FC state.

Comparison of the TRIR spectrum of Ag-Cyd after correction for the hot D_2O signal with the TRIR spectrum of $Ag-dC_{20}$ at 2000 ps shows that they both exhibit a peak near 1580 cm⁻¹, although this peak is 10-fold weaker in Ag-Cyd (**Figure 3**). The very weak band at 1580 cm⁻¹ in the Ag-Cyd TRIR spectra, which can only be seen after extensive signal averaging, precludes the observation of the rise that is so prominent in the Ag-dC₂₀ signal kinetics (**Figure 4**, red circles). Nonetheless, the similar long-time signals indicate that the triplet excimer state is formed in both systems.

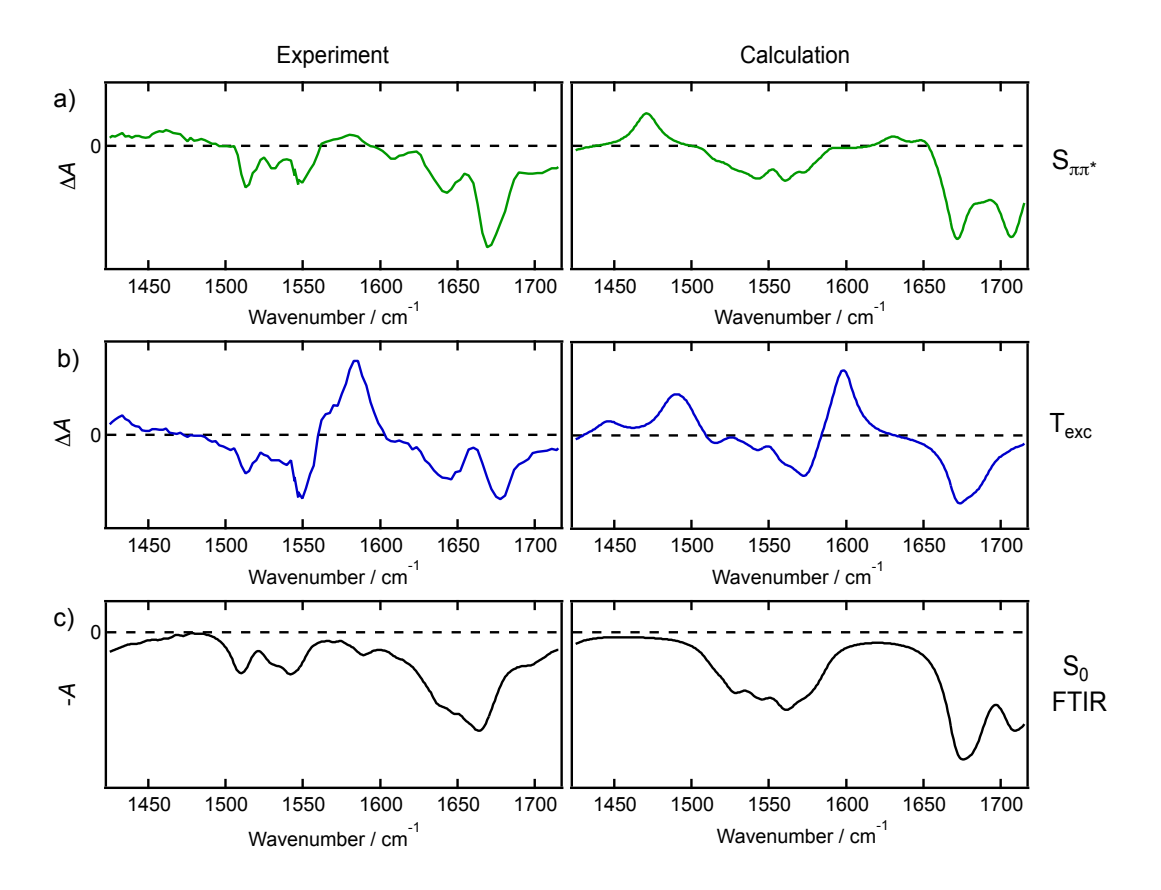


Figure 7. (a, b) Species associated difference spectra (SADS) extracted from the Ag-dC₂₀ TRIR data (left) compared with the calculated difference spectra from quantum mechanical calculations on the Ag₂(dC₂)₂ model duplex (right). Each species is labeled on the right and corresponds to the following electronic states: (a) $S_{\pi\pi^*}$ and (b) T_{exc} state. (c) Experimental IR absorption spectrum of Ag-dC₂₀ (left) compared with the calculated IR absorption spectrum of Ag₂(dC₂)₂ on the right (both curves have been inverted for better comparison with the upper panels).

The 10-fold weaker long-time signal in Ag-Cyd is explained by the lower prevalence of the requisite supramolecular motifs for populating the triplet excimer state. Even though the concentration of Cyd in the Ag-Cyd solution is four times greater than in Ag-dC₂₀, the lack of a covalent polymer backbone disfavors the stacking aggregation that is proposed to be necessary for forming the gateway CT state that leads to the $T_{\rm exc}$ state. We

suggest that the Ag-Cyd sample produces similar self-assembly motifs as the Ag-dC $_{20}$ sample except at a lower abundance due to the lack of a covalent backbone. This is supported by the appearance of a weak component in the CD spectrum of Ag-Cyd

(**Figure S8b**) that matches the dual negative bands seen in the CD spectrum of Ag-dC₂₀ (**Figure 2c** in ref.¹⁹).

The 1586 cm⁻¹ band that is prominent in Ag-dC₂₀ (**Figure 2a**) and barely detectable in Ag-Cyd (Figure 3) vanishes altogether in the TRIR spectrum of Ag-Cyt (Figure S3c). We rule out a heavy atom effect as the cause of the enhanced ISC observed in the first two systems because all three systems have bound silver ions and C-Ag+-C base pairs. We suggest that the propeller twisted base pair geometry plays a key role in the formation of the triplet excimer state. This geometry, which is absent for Ag-Cyt in D₂O, enables access to the CT state that is the gateway state to the T_{exc} state. Crystals grown from a AgNO₃ and cytosine solution have sheets of Cyt-Ag+-Cyt base pairs with minimal twisting.⁵⁰ Significantly, the gateway CT state does not involve CT between cytosines. Indeed, the lowest vertical transition to an excited state with strong CT character is the seventh singlet excited state of Ag₂(dC₂)₂ (**Table S2**). Instead, the calculations suggest that partial CT occurs from the silver ion to a cytosine in a twisted C-Ag+-C base pair. Partial CT is inhibited in the nearly planar C-Ag+-C base pairs, explaining why the gateway CT state is absent in the Ag(Cyt)₂ model (**Figure 6b**).

C. Photochemical Impacts of Ag+ binding

The photochemical possibilities of a triplet excimer state are considered in this section. Triplet-mediated thymine-thymine CPD formation has been studied intensely due to its relatively low triplet energy,⁵⁸⁻⁶¹ high triplet yield,⁶²⁻⁶⁵ and high CPD yield.⁶⁶⁻⁶⁷ Formation of CPDs via triplet states in thymine has been proposed to involve a biradical intermediate, which can decay to the ground state or form CPDs.⁶⁸⁻⁷² Studies of thymine systems by Zinth and coworkers^{68, 72-73} identified a triplet thymine biradical with 4% of the population forming CPDs and 96% re-forming the ground state.^{68, 73}

Because past computational studies have suggested that triplet excimers are the precursors to these biradicals, $^{25, 31, 74}$ we hypothesized that UV-irradiated Ag-dC₂₀ would undergo extensive photochemical damage. However, we observed minimal photodegradation in keeping with the observation that irradiating DNA or poly(rC) at room temperature in the presence of silver ions does not enhance cytosine-cytosine CPD formation. In contrast, Rahn and Landry reported that the yield of TT CPDs increases 20-fold when Ag*-bound poly(dT) is irradiated by UV light.⁵⁶

Our computational results suggest why CPD formation is disfavored in Ag-dC₂₀. $T_{\rm exc}$ is suggested to be non-reactive because ground state recovery is favored over CPD formation (**Figure S6**). Because previous calculations of a stacked cytosine dimer³¹ and i-motif structures,⁷⁵ without metal ions suggested the opposite, we studied how Ag+ ion complexation affects the photoreactivity. We repeated all calculations starting from the $T_{\rm exc}$ state, but with the Ag+ ions removed. Although the pathway is slightly favored in this case (i.e., the energy barrier to access the T_1/S_0 funnel disappears), CPD formation is still disfavored. We conclude that the structural rearrangements induced by the Ag+ ions disfavor CPD photoreactivity compared to "natural" face-to-face dispositions.

4. CONCLUSIONS

The TRIR spectra and computational results presented in this study provide the first evidence of a triplet excimer state in a metallo-DNA system. To the best of our knowledge, a cytosine-

based triplet state has not been detected previously in a DNA oligonucleotide by time-resolved spectroscopy. Pyrimidine triplet excimers have been discussed as short-lived intermediates for CPD formation in DNA but the triplet excimer state detected here in the Ag-dC20 metallo-DNA persists into the ns timescale and is photochemically unreactive. Although CPDs do not appear to form, further study of the triplet excimer state is needed, especially with an eye toward determining whether this long-lived triplet state with an energy of 1.6 eV is capable of photosensitizing damage through singlet oxygen generation. If this turns out to be the case, then it would constitute a new damage pathway for DNA or DNA nanostructures that contain coordinated silver ions.

Our study, which focused on identifying the long-lived excited state and its precursor, does not address the dynamics that take place on faster timescales. Although there is substantial temporal and spectral congestion, future work may bring clarity to the initial excited state dynamics that are suggested by the potential energy landscape, including the putative branching that occurs from the initial Franck-Condon region to excimer states of singlet and triplet multiplicity.

The observation of a triplet excimer state in Ag-dC₂₀, which is seen only very weakly in Ag-Cyd, and not at all in Ag-Cyt, points to the importance of supramolecular interactions among two or more C-Ag⁺-C base pairs. All three systems have C-Ag⁺-C base pairs as inferred from their IR spectra, but this motif does not lead on its own to a triplet excimer state, ruling out a heavy atom effect induced by silver ion binding. Instead, our results implicate the propeller twisted base pairs that are the distinctive motif of self-assembled structures made of stacked C-Ag⁺-C base pairs. As this study shows, understanding excited state decay pathways in complex supramolecular systems, including metal-mediated DNA nanostructures, is increasingly feasible through the powerful combination of time-resolved vibrational spectroscopy and QM calculations.

5. METHODS

5.1. Sample preparation. All experiments were performed on D_2O solutions. The compounds, dC_{20} (Midland Reagent Company), cytosine (Sigma Aldrich), cytidine (Sigma Aldrich), and AgNO₃ (Sigma Aldrich) were used as received. dC_{20} was purified using gel-filtration by the supplier and delivered as a lyophilized solid. Single-stranded dC_{20} (ss- dC_{20}) samples were prepared by adding 540 nmol of dC_{20} to 2 mL of D_2O to yield a concentration of 5.4 mM in cytosine residues. All concentrations of oligonucleotides are in moles of mononucleotides per unit volume. The number of moles of cytosine in dC_{20} was quantified by the supplier using the absorbance of the sample in aqueous solution at 260 nm and an extinction coefficient for dC of 7400 M^{-1} cm⁻¹.76

The Ag- dC_{20} solution was prepared by adding concentrated $AgNO_3$ solution to a ss- dC_{20} solution. The initial concentrations of Ag^+ ion and cytosine residues were 2.7 mM and 5.4 mM, respectively, corresponding to a Ag^+ -to-nucleobase ratio, defined as β , of 0.5. The concentrations used to calculate β are the initial or total concentrations. For this reason, β may differ from the silver ion-nucleobase stoichiometry for some complexes. The pD (= $-log_{10}[D_3O^+]$) was adjusted for some measurements by adding small drops of concentrated DNO₃ or NaOD in D_2O (Sigma-Aldrich). pD values were determined by adding 0.4 to the readout of a glass electrode pH meter.

Cyd solutions were prepared by dissolving lyophilized cytidine solid in unbuffered D_2O to yield a concentration of 20.2 mM. Ag-Cyd samples were prepared by adding concentrated AgNO₃ to the unbuffered Cyd D_2O solution to yield formal concentrations of 10.1 mM AgNO₃ and 20.2 mM Cyd (β = 0.5). The same concentrations were used for the cytosine monomer and Ag-Cyt solutions. Higher concentrations of the Cyt and Cyd monomers were used to ensure that nearly all silver ions are bound as explained in ref. ¹⁹.

Special care was taken to minimize the amount of unbound Ag^+ in solution. The presence of free Ag^+ results in broad positive TRIR signals which continually rise in amplitude over time (**Figure S10a**) and leaves dark deposits on the CaF_2 windows, which we attribute to reduced silver clusters. These artifacts can be avoided by adding the metal ion-chelator ethylenediaminetetraacetic acid (EDTA) (**Figure S10b,c**). All data in this study were recorded without added EDTA because satisfactory results were obtained by adding only as much $AgNO_3$ as needed to produce $\beta = 0.5$ solutions, thereby avoiding free silver ions.

- **5.2. Steady-state spectroscopy.** IR absorption spectra were recorded using an FTIR spectrometer (FT/IR-4200, JASCO) as the average of 64 scans with a spectral resolution of 4 cm⁻¹. All samples were measured in a static cell in which a 100 μm thick Teflon spacer was sandwiched between two CaF₂ plates. Circular Dichroism (CD) and UV-vis spectra of solutions held in a 100 μm fused silica cell were recorded using a JASCO J-815 CD spectrometer. Spectra were obtained by averaging two scans recorded at a scan speed of 100 nm min⁻¹ and a bandwidth of 1 nm.
- **5.3. Time-resolved infrared spectroscopy.** TRIR measurements were performed with a previously described setup.⁷⁷ A Ti:Sapphire amplified fs laser system (Libra-HE, Coherent Inc.) was used to generate 265 nm pump pulses from an OPA (OPerA Solo, Coherent Inc). A second OPA (TOPAS with nDFG, Coherent Inc.) generated probe pulses with center wavelengths of 6150 nm and 6800 nm. The probe pulses were separated into signal and reference beams. which were focused to spatially separated spots on the sample, and only the pump beam was overlapped with the signal beam. The probe beam polarization was set to be 54.7° relative to the pump beam. Both the signal and reference beams were dispersed onto a liquid N2-cooled 64-element HgCdTe detector. The sample was recirculated in a CaF2 cell with a 100 µm spacer. The pump beam, with a pump energy of 3.6 μJ, was focused to a spot with a 560 μm $1/e^2$ radius, resulting in a peak fluence of $730 \pm 120 \mu J \text{ cm}^{-2}$ at the sample. Global fitting was performed using the GloTarAn (legacy) program. The uncertainties in the time constants represent twice the standard error from fitting.

6. Computational Methods

The ground state structure of Ag(Cyt)₂ was optimized using density functional theory (DFT), with the M052X functional, ⁷⁸⁻⁷⁹ the def2-svp basis set, and a pseudopotential for Ag⁺.⁸⁰ Bulk solvent effects were included using the Polarizable Continuum Model (PCM). ⁸¹⁻⁸² Excited state vertical absorption energies (VAEs), potential energy surfaces (PES) and infrared spectra (IR) were mapped, resorting to the time-dependent version of DFT (TD-DFT). The larger Ag₂(dC₂)₂ structure was divided in two regions, a QM part consisting of the nucleobases and Ag⁺ atoms described with the method specified above, and the sugar, connecting backbone, and external ions that were computed at the MM level (amber force field parm96.dat). ⁸³ Both regions were coupled using the ONIOM⁸⁴ interface as implemented in Gaussian16. ⁸⁵ Complete Active Space Self-Consistent Field (CASSCF)⁸⁶ calculations were

also performed with OpenMolcas⁸⁷ to estimate the Spin Orbit Coupling (SOC) terms in the model systems. The molecular orbitals that constitute the active space for the CASSCF calculations are displayed in **Figures S11** – **S13.** More details are given in supplementary material.

ASSOCIATED CONTENT

Supporting Information

See the supplementary material for information on effects of adding ethylenediaminetetraacetic acid (EDTA) to dC_{20} solutions with Cyt:Ag+ < 2:1, steady state spectra of Cyt/Ag-Cyt and Cyd/Ag-Cyd, raw calculated IR spectra, UV-Vis of TRIR samples and further computational details and discussion.

ACKNOWLEDGMENT

Work at The Ohio State University was supported by a grant from the US National Science Foundation (CHE-1800471). L.M.F. thanks the Madrid Government (Comunidad de Madrid-Spain) under the Multiannual Agreement with Universidad Autónoma de Madrid in the line Support to Young Researchers, in the context of the V PRICIT (Regional Programme of Research and Technological Innovation) (SI3/PJI/2021-00331) and the Centro de Computación Científica UAM (CCC-UAM) for computing time. The authors declare no competing financial interests.

REFERENCES

- 1. Sigel, R. K. O.; Sigel, H., A Stability Concept for Metal Ion Coordination to Single-Stranded Nucleic Acids and Affinities of Individual Sites. *Acc. Chem. Res.* **2010**, *43* (7), 974-984.
- 2. Takezawa, Y.; Shionoya, M., Supramolecular DNA Three-Way Junction Motifs With a Bridging Metal Center. *Front. Chem.* **2020,** *7*.
- 3. Choi, S.; Dickson, R. M.; Yu, J., Developing luminescent silver nanodots for biological applications. *Chem. Soc. Rev.* **2012.** *41* (5). 1867-1891.
- 4. Zhou, W.; Saran, R.; Liu, J., Metal Sensing by DNA. *Chem. Rev.* **2017**, *117* (12), 8272-8325.
- 5. Nagraj, N.; Lu, Y., Catalytic Nucleic Acid Biosensors for Environmental Monitoring. In Nucleic Acid Biosensors for Environmental Pollution Monitoring; Royal Society of Chemistry, 2011; pp 82–98.
- 6. Bloomfield, V. A., DNA condensation. *Curr. Opin. Struct. Biol.* **1996,** *6* (3), 334-341.
- 7. Clever, G. H.; Kaul, C.; Carell, T., DNA-Metal Base Pairs. *Angew. Chem. Int. Ed.* **2007**, *46* (33), 6226-6236.
- 8. Tanaka, Y.; Kondo, J.; Sychrovský, V.; Šebera, J.; Dairaku, T.; Saneyoshi, H.; Urata, H.; Torigoe, H.; Ono, A., Structures, physicochemical properties, and applications of T–Hg^{II}–T, C–Ag^I–C, and other metallo-base-pairs. *Chem. Commun.* **2015**, *51* (98), 17343-17360.
- 9. Takezawa, Y.; Müller, J.; Shionoya, M., Artificial DNA Base Pairing Mediated by Diverse Metal Ions. *Chem. Lett.* **2016**, *46* (5), 622-633.

- 10. Naskar, S.; Guha, R.; Müller, J., Metal-Modified Nucleic Acids: Metal-Mediated Base Pairs, Triples, and Tetrads. *Angew. Chemie Int. Ed.* **2020**, *59* (4), 1397-1406.
- 11. Gonzàlez-Rosell, A.; Cerretani, C.; Mastracco, P.; Vosch, T.; Copp, S. M., Structure and Luminescence of DNA-templated Silver Clusters. *Nanoscale Adv.* **2021**, *3* (5), 1230-1260.
- 12. Hollenstein, M., DNA Catalysis: The Chemical Repertoire of DNAzymes *Molecules* **2015**, *20* (11), 20777-20804.
- 13. Roelfes, G.; Boersma, A. J.; Feringa, B. L., Highly enantioselective DNA-based catalysis. *Chem. Commun.* **2006**, (6), 635-637.
- 14. McConnell, E. M.; Cozma, I.; Mou, Q.; Brennan, J. D.; Lu, Y.; Li, Y., Biosensing with DNAzymes. *Chem. Soc. Rev.* **2021**, *50* (16), 8954-8994.
- 15. Díez, I.; Ras, R. H. A., Fluorescent Silver Nanoclusters. *Nanoscale* **2011**, *3* (5), 1963-1970.
- 16. Latorre, A.; Somoza, Á., DNA-Mediated Silver Nanoclusters: Synthesis, Properties and Applications. *ChemBioChem* **2012**, *13* (7), 951-958.
- 17. Huard, D. J. E.; Demissie, A.; Kim, D.; Lewis, D.; Dickson, R. M.; Petty, J. T.; Lieberman, R. L., Atomic Structure of a Fluorescent Ag₈ Cluster Templated by a Multistranded DNA Scaffold. *J. Am. Chem. Soc.* **2019**, *141* (29), 11465-11470.
- 18. Zhang, Y.; He, C.; Petty, J. T.; Kohler, B., Time-Resolved Vibrational Fingerprints for Two Silver Cluster-DNA Fluorophores. *J. Phys. Chem. Lett.* **2020**, *11* (21), 8958-8963.
- 19. Kohl, F. R.; Zhang, Y.; Charnay, A. P.; Martínez-Fernández, L.; Kohler, B., Ultrafast Excited State Dynamics of Silver Ion-Mediated Cytosine–Cytosine Base Pairs In Metallo-DNA. *J. Chem. Phys.* **2020**, *153* (10), 105104.
- 20. Crespo-Hernández, C. E.; Cohen, B.; Hare, P. M.; Kohler, B., Ultrafast Excited-State Dynamics in Nucleic Acids. *Chem. Rev.* **2004**, *104* (4), 1977-2020.
- 21. Middleton, C. T.; de La Harpe, K.; Su, C.; Law, Y. K.; Crespo-Hernández, C. E.; Kohler, B., DNA Excited-State Dynamics: From Single Bases to the Double Helix. *Annu. Rev. Phys. Chem.* **2009**, *60* (1), 217-239.
- 22. Improta, R.; Santoro, F.; Blancafort, L., Quantum Mechanical Studies on the Photophysics and the Photochemistry of Nucleic Acids and Nucleobases. *Chem. Rev.* **2016**, *116* (6), 3540-3593.
- 23. Gustavsson, T.; Markovitsi, D., Fundamentals of the Intrinsic DNA Fluorescence. *Acc. Chem. Res.* **2021,** *54* (5), 1226-1235.
- 24. Martínez Fernández, L.; Santoro, F.; Improta, R., Nucleic Acids as a Playground for the Computational Study of the Photophysics and Photochemistry of Multichromophore Assemblies. *Acc. Chem. Res.* **2022**, *55* (15), 2077-2087.
- 25. Cuquerella, M. C.; Lhiaubet-Vallet, V.; Bosca, F.; Miranda, M. A., Photosensitised Pyrimidine Dimerisation in DNA. *Chem. Sci.* **2011**, *2* (7), 1219-1232.
- 26. Cadet, J.; Mouret, S.; Ravanat, J. L.; Douki, T., Photoinduced damage to cellular DNA: direct and

- photosensitized reactions. *Photochem. Photobiol.* **2012**, *88* (5), 1048-65.
- 27. Miranda, M. A.; Lhiaubet-Vallet, V., Triplet Channel Photochemistry in DNA. In *DNA Photodamage: From Light Absorption to Cellular Responses and Skin Cancer*, The Royal Society of Chemistry: 2022; pp 55-76.
 28. Funai, T.; Aotani, M.; Kiriu, R.; Nakamura, J.; Miyazaki, Y.; Nakagawa, O.; Wada, S.; Torigoe, H.; Ono, A.;
- Miyazaki, Y.; Nakagawa, O.; Wada, S.; Torigoe, H.; Ono, A.; Urata, H., Silver(I)-Ion-Mediated Cytosine-Containing Base Pairs: Metal Ion Specificity for Duplex Stabilization and Susceptibility toward DNA Polymerases. *ChemBioChem* **2020**, *21* (4), 517-522.
- 29. Vecchioni, S.; Capece, M. C.; Toomey, E.; Nguyen, L.; Ray, A.; Greenberg, A.; Fujishima, K.; Urbina, J.; Paulino-Lima, I. G.; Pinheiro, V.; Shih, J.; Wessel, G.; Wind, S. J.; Rothschild, L., Construction and characterization of metal ion-containing DNA nanowires for synthetic biology and nanotechnology. *Sci. Rep.* **2019**, *9* (1), 6942.
- 30. Fardian-Melamed, N.; Katrivas, L.; Eidelshtein, G.; Rotem, D.; Kotlyar, A.; Porath, D., Electronic Level Structure of Silver-Intercalated Cytosine Nanowires. *Nano Lett.* **2020**, *20* (6), 4505-4511.
- 31. Roca-Sanjuán, D.; Olaso-González, G.; González-Ramírez, I.; Serrano-Andrés, L.; Merchán, M., Molecular Basis of DNA Photodimerization: Intrinsic Production of Cyclobutane Cytosine Dimers. *J. Am. Chem. Soc.* **2008**, *130* (32), 10768-10779.
- 32. Keane, P. M.; Wojdyla, M.; Doorley, G. W.; Watson, G. W.; Clark, I. P.; Greetham, G. M.; Parker, A. W.; Towrie, M.; Kelly, J. M.; Quinn, S. J., A Comparative Picosecond Transient Infrared Study of 1-Methylcytosine and 5'-dCMP That Sheds Further Light on the Excited States of Cytosine Derivatives. *J. Am. Chem. Soc.* **2011**, *133* (12), 4212-4215.
- 33. Penfold, T. J.; Gindensperger, E.; Daniel, C.; Marian, C. M., Spin-Vibronic Mechanism for Intersystem Crossing. *Chem. Rev.* **2018**, *118* (15), 6975-7025.
- 34. Spata, V. A.; Matsika, S., Bonded Excimer Formation in π -Stacked 9-Methyladenine Dimers. *J. Phys. Chem. A.* **2013**, *117* (36), 8718-8728.
- 35. Wang, Y.; Haze, O.; Dinnocenzo, J. P.; Farid, S.; Farid, R. S.; Gould, I. R., Bonded Exciplexes. A New Concept in Photochemical Reactions. *The Journal of Organic Chemistry* **2007**, *72* (18), 6970-6981.
- 36. Martínez-Fernández, L.; Pepino, A. J.; Segarra-Martí, J.; Jovaišaitė, J.; Vaya, I.; Nenov, A.; Markovitsi, D.; Gustavsson, T.; Banyasz, A.; Garavelli, M.; Improta, R., Photophysics of Deoxycytidine and 5-Methyldeoxycytidine in Solution: A Comprehensive Picture by Quantum Mechanical Calculations and Femtosecond Fluorescence Spectroscopy. *J. Am. Chem. Soc.* **2017**, *139* (23), 7780-7791.
- 37. Gehring, K.; Leroy, J.-L.; Guéron, M., A tetrameric DNA structure with protonated cytosine-cytosine base pairs. *Nature* **1993**, *363* (6429), 561-565.
- 38. Mergny, J.-L.; Sen, D., DNA Quadruple Helices in Nanotechnology. *Chem. Rev.* **2019**, *119* (10), 6290-6325.
- 39. Lippert, B., Alterations of Nucleobase pK_a Values upon Metal Coordination: Origins and Consequences. In

- *Prog. Inorg. Chem.*; John Wiley & Sons, Ltd, **2005**; pp 385–447.
- 40. Banyay, M.; Sarkar, M.; Gräslund, A., A Library of IR bands of Nucleic Acids in Solution. *Biophys. Chem.* **2003**, *104* (2), 477-488.
- 41. Peng, C. S.; Jones, K. C.; Tokmakoff, A., Anharmonic Vibrational Modes of Nucleic Acid Bases Revealed by 2D IR Spectroscopy. *J. Am. Chem. Soc.* **2011**, *133* (39), 15650-15660.
- 42. Dai, Q.; Sanstead, P. J.; Peng, C. S.; Han, D.; He, C.; Tokmakoff, A., Weakened N3 Hydrogen Bonding by 5-Formylcytosine and 5-Carboxylcytosine Reduces Their Base-Pairing Stability. *ACS Chem. Biol.* **2016**, *11* (2), 470-477.
- 43. Florián, J.; Baumruk, V.; Leszczyński, J., IR and Raman Spectra, Tautomeric Stabilities, and Scaled Quantum Mechanical Force Fields of Protonated Cytosine. *J. Phys. Chem.* **1996**, *100* (13), 5578-5589.
- 44. Geinguenaud, F.; Liquier, J.; Brevnov, M. G.; Petrauskene, O. V.; Alexeev, Y. I.; Gromova, E. S.; Taillandier, E., Parallel Self-Associated Structures Formed by T,C-Rich Sequences at Acidic pH. *Biochemistry* **2000**, *39* (41), 12650-12658.
- 45. Keane, P. M.; Baptista, F. R.; Gurung, S. P.; Devereux, S. J.; Sazanovich, I. V.; Towrie, M.; Brazier, J. A.; Cardin, C. J.; Kelly, J. M.; Quinn, S. J., Long-Lived Excited-State Dynamics of i-Motif Structures Probed by Time-Resolved Infrared Spectroscopy. *ChemPhysChem* **2016**, *17* (9), 1281-1287.
- 46. Keane, P. M.; Wojdyla, M.; Doorley, G. W.; Kelly, J. M.; Parker, A. W.; Clark, I. P.; Greetham, G. M.; Towrie, M.; Magno, L. M.; Quinn, S. J., Long-lived Excited States in imotif DNA Studied by Picosecond Time-Resolved IR Spectroscopy. *Chem. Commun.* **2014**, *50* (23), 2990-2992.
- 47. Swasey, S. M.; Rosu, F.; Copp, S. M.; Gabelica, V.; Gwinn, E. G., Parallel Guanine Duplex and Cytosine Duplex DNA with Uninterrupted Spines of Ag¹-Mediated Base Pairs. *I. Phys. Chem. Lett.* **2018**, 9 (22), 6605-6610.
- 48. Espinosa Leal, L. A.; Karpenko, A.; Swasey, S.; Gwinn, E. G.; Rojas-Cervellera, V.; Rovira, C.; Lopez-Acevedo, O., The Role of Hydrogen Bonds in the Stabilization of Silver-Mediated Cytosine Tetramers. *J. Phys. Chem. Lett.* **2015**, *6* (20), 4061-4066.
- 49. Megger, D. A.; Fonseca Guerra, C.; Bickelhaupt, F. M.; Müller, J., Silver(I)-Mediated Hoogsteen-Type base pairs. *J. Inorg. Biochem.* **2011**, *105* (11), 1398-1404.
- 50. Mistry, L.; Waddell, P. G.; Wright, N. G.; Horrocks, B. R.; Houlton, A., Transoid and Cisoid Conformations in Silver-Mediated Cytosine Base Pairs: Hydrogen Bonding Dictates Argentophilic Interactions in the Solid State. *Inorg. Chem.* **2019**, *58* (19), 13346-13352.
- 51. Mistry, L.; El-Zubir, O.; Dura, G.; Clegg, W.; Waddell, P. G.; Pope, T.; Hofer, W. A.; Wright, N. G.; Horrocks, B. R.; Houlton, A., Addressing the Properties of "Metallo-DNA" With a Ag(I)-Mediated Supramolecular Duplex. *Chem. Sci.* **2019**, *10* (11), 3186-3195.
- 52. Linares, F.; García-Fernández, E.; López-Garzón, F. J.; Domingo-García, M.; Orte, A.; Rodríguez-Diéguez, A.;

- Galindo, M. A., Multifunctional Behavior of Molecules Comprising Stacked Cytosine–Agl–Cytosine Base Pairs; Towards Conducting and Photoluminescence Silver-DNA Nanowires. *Chem. Sci.* **2019**, *10* (4), 1126-1137.
- 53. Goncharova, I., Ag(I)-Mediated Homo and Hetero Pairs of Guanosine and Cytidine: Monitoring by Circular Dichroism Spectroscopy. *Spectrochim. Acta, Part A* **2014**, *118*, 221-227.
- 54. Schreier, W. J.; Schrader, T. E.; Koller, F. O.; Gilch, P.; Crespo-Hernández, C. E.; Swaminathan, V. N.; Carell, T.; Zinth, W.; Kohler, B., Thymine Dimerization in DNA Is an Ultrafast Photoreaction. *Science* **2007**, *315* (5812), 625-629.
- 55. Quinn, S.; Doorley, G. W.; Watson, G. W.; Cowan, A. J.; George, M. W.; Parker, A. W.; Ronayne, K. L.; Towrie, M.; Kelly, J. M., Ultrafast IR Spectroscopy of the Short-Lived Transients formed by UV Excitation of Cytosine Derivatives. *Chem. Commun.* **2007**, (21), 2130-2132.
- 56. Rahn, R. O.; Landry, L. C., Ultraviolet Irradiation of Nucleic Acids Complexed with Heavy Atoms-II. Phosphorescence and Photodimerization of DNA Complexes with Ag. *Photochem. Photobiol.* **1973**, *18* (1), 29-38.
- 57. van Stokkum, I. H. M.; Larsen, D. S.; van Grondelle, R., Global and Target Analysis of Time-Resolved Spectra. *Biochim. Biophys. Acta Bioenerg.* **2004**, *1657* (2-3), 82-104.
- 58. Bosca, F.; Lhiaubet-Vallet, V.; Cuquerella, M. C.; Castell, J. V.; Miranda, M. A., The Triplet Energy of Thymine in DNA. *J. Am. Chem. Soc.* **2006**, *128* (19), 6318-6319.
- 59. Wood, P. D.; Redmond, R. W., Triplet State Interactions between Nucleic Acid Bases in Solution at Room Temperature: Intermolecular Energy and Electron Transfer. *J. Am. Chem. Soc.* **1996,** *118* (18), 4256-4263.
- 60. Merchán, M.; Serrano-Andrés, L.; Robb, M. A.; Blancafort, L., Triplet-State Formation along the Ultrafast Decay of Excited Singlet Cytosine. *J. Am. Chem. Soc.* **2005**, *127* (6), 1820-1825.
- 61. Abouaf, R.; Pommier, J.; Dunet, H.; Quan, P.; Nam, P.-C.; Nguyen, M. T., The Triplet State of Cytosine and its Derivatives: Electron Impact and Quantum Chemical Study. *J. Chem. Phys.* **2004**, *121* (23), 11668-11674.
- 62. Lamola, A. A.; Eisinger, J., Excited States of Nucleotides in Water at Room Temperature. *Biochim. Biophys. Acta* **1971**, *240* (3), 313-325.
- 63. Salet, C.; Bensasson, R.; Becker, R. S., Triplet Excited States of Pyrimidine Nucleosides and Nucleotides. *Photochem. Photobiol.* **1979**, *30* (3), 325-329.
- 64. Salet, C.; Bensasson, R., Studies on Thymine and Uracil Triplet Excited State in Acetonitrile and Water. *Photochem. Photobiol.* **1975**, *22* (6), 231-235.
- 65. Fisher, G. J.; Johns, H. E., Ultraviolet Photochemistry of Thymine in Aqueous Solution. *Photochem. Photobiol.* **1970**, *11* (6), 429-444.

- 66. Cadet, J.; Vigny, P., The Photochemistry of Nucleic Acids. In *Bioorganic Photochemistry*, Morrison, H., Ed. Wiley: New York, 1990; Vol. 1, pp 3-40.
- 67. Gueron, M.; Eisinger, J.; Lamola, A., Basic Principles in Nucleic Acid Chemistry. **1974**.
- 68. Pilles, B. M.; Bucher, D. B.; Liu, L.; Gilch, P.; Zinth, W.; Schreier, W. J., Identification of Charge Separated States in Thymine Single Strands. *Chem. Commun.* **2014**, *50* (98), 15623-15626.
- 69. Wagner, P. J.; Bucheck, D. J., Causes for the Low Efficiency of Thymine and Uracil Photodimerization in Solution. *J. Am. Chem. Soc.* **1968**, *90* (23), 6530-6532.
- 70. Durbeej, B.; Eriksson, L. A., Reaction Mechanism of Thymine Dimer Formation in DNA Induced by UV Light. *J. Photochem. Photobiol. A: Chem.* **2002**, *152* (1), 95-101.
- 71. Zhang, R. B.; Eriksson, L. A., A Triplet Mechanism for the Formation of Cyclobutane Pyrimidine Dimers in UV-Irradiated DNA. *J. Phys. Chem. B.* **2006**, *110* (14), 7556-7562.
- 72. Gontcharov, J.; Liu, L.; Pilles, B. M.; Carell, T.; Schreier, W. J.; Zinth, W., Triplet-Induced Lesion Formation at CpT and TpC Sites in DNA. *Chem. Eur. J.* **2019**, *25* (66), 15164-15172.
- 73. Liu, L.; Pilles, B. M.; Gontcharov, J.; Bucher, D. B.; Zinth, W., Quantum Yield of Cyclobutane Pyrimidine Dimer Formation Via the Triplet Channel Determined by Photosensitization. *J. Phys. Chem. B.* **2016**, *120* (2), 292-298.
- 74. Climent, T.; González-Ramírez, I.; González-Luque, R.; Merchán, M.; Serrano-Andrés, L., Cyclobutane Pyrimidine Photodimerization of DNA/RNA Nucleobases in the Triplet State. *J. Phys. Chem. Lett.* **2010**, *1* (14), 2072-2076.
- 75. Improta, R. Shedding Light on the Photophysics and Photochemistry of I-Motifs Using Quantum Mechanical Calculations *International Journal of Molecular Sciences* [Online], 2023.
- 76. Cantor, C. R.; Warshaw, M. M.; Shapiro, H., Oligonucleotide Interactions. 3. Circular Dichroism Studies of the Conformation of Deoxyoligonucleotides. *Biopolymers* **1970**, *9* (9), 1059-1077.
- 77. Zhang, Y.; Chen, J.; Kohler, B., Hydrogen Bond Donors Accelerate Vibrational Cooling of Hot Purine Derivatives in Heavy Water. *J. Phys. Chem. A.* **2013**, *117* (31), 6771-6780.
- 78. Zhao, Y.; Schultz, N. E.; Truhlar, D. G., Design of Density Functionals by Combining the Method of Constraint Satisfaction with Parametrization for Thermochemistry, Thermochemical Kinetics, and Noncovalent Interactions. *J. Chem. Theory Comput.* **2006**, *2* (2), 364-382.
- 79. Zhao, Y.; Truhlar, D. G., Density Functionals with Broad Applicability in Chemistry. *Acc. Chem. Res.* **2008**, *41* (2), 157-167.
- 80. Andrae, D.; Häußermann, U.; Dolg, M.; Stoll, H.; Preuß, H., Energy-Adjusted *Ab Initio* Pseudopotentials for the Second and Third Row Transition Elements. *Theor. Chim. Acta* **1990**, *77* (2), 123-141.

- 81. Miertuš, S.; Scrocco, E.; Tomasi, J., Electrostatic Interaction of a Solute with a Continuum. A Ddirect Utilizaion of *ab initio* Molecular Potentials for the Prevision of Solvent Effects. *Chem. Phys.* **1981**, *55* (1), 117-129.
- 82. Tomasi, J.; Mennucci, B.; Cammi, R., Quantum Mechanical Continuum Solvation Models. *Chem. Rev.* **2005**, *105* (8), 2999-3093.
- 83. Cornell, W. D.; Cieplak, P.; Bayly, C. I.; Gould, I. R.; Merz, K. M.; Ferguson, D. M.; Spellmeyer, D. C.; Fox, T.; Caldwell, J. W.; Kollman, P. A., A Second Generation Force Field for the Simulation of Proteins, Nucleic Acids, and Organic Molecules. *J. Am. Chem. Soc.* **1995**, *117* (19), 5179-5197.
- 84. Dapprich, S.; Komáromi, I.; Byun, K. S.; Morokuma, K.; Frisch, M. J., A New ONIOM Implementation in Gaussian 98. Part I. The Calculation of Energies, Gradients, Vibrational Frequencies and Electric Field Derivatives. *J. Mol. Struc.: THEOCHEM* **1999**, 461-462, 1-21.
- 85. Frisch, M. J.; Trucks, G. W.; Schlegel, H. B.; Scuseria, G. E.; Robb, M. A.; Cheeseman, J. R.; Scalmani, G.; Barone, V.: Petersson, G. A.; Nakatsuji, H.; Li, X.; Caricato, M.; Marenich, A. V.; Bloino, J.; Janesko, B. G.; Gomperts, R.; Mennucci, B.; Hratchian, H. P.; Ortiz, J. V.; Izmaylov, A. F.; Sonnenberg, J. L.; Williams; Ding, F.; Lipparini, F.; Egidi, F.; Goings, J.; Peng, B.; Petrone, A.; Henderson, T.; Ranasinghe, D.; Zakrzewski, V. G.; Gao, J.; Rega, N.; Zheng, G.; Liang, W.; Hada, M.; Ehara, M.; Toyota, K.; Fukuda, R.; Hasegawa, J.; Ishida, M.; Nakajima, T.; Honda, Y.; Kitao, O.; Nakai, H.; Vreven, T.; Throssell, K.; Montgomery Jr., J. A.; Peralta, J. E.; Ogliaro, F.; Bearpark, M. J.; Heyd, J. J.; Brothers, E. N.; Kudin, K. N.; Staroverov, V. N.; Keith, T. A.; Kobayashi, R.; Normand, J.; Raghavachari, K.; Rendell, A. P.; Burant, J. C.; Ivengar, S. S.; Tomasi, J.; Cossi, M.; Millam, J. M.; Klene, M.; Adamo, C.; Cammi, R.; Ochterski, J. W.; Martin, R. L.; Morokuma, K.; Farkas, O.; Foresman, J. B.; Fox, D. J. Gaussian 16 Rev. B.01, Wallingford, CT, 2016.
- 86. Roos, B. O.; Lawley, K., *Ab initio* Methods in Quantum Chemistry II. *Adv. Chem. Phys.* **1987**, *69*, 399-446.
- Fdez. Galván, I.; Vacher, M.; Alavi, A.; Angeli, C.; Aguilante, F.; Autschbach, J.; Bao, J. J.; Bokarev, S. I.; Bogdanov, N. A.; Carlson, R. K.; Chibotaru, L. F.; Creutzberg, J.; Dattani, N.; Delcey, M. G.; Dong, S. S.; Dreuw, A.; Freitag, L.; Frutos, L. M.; Gagliardi, L.; Gendron, F.; Giussani, A.; González, L.; Grell, G.; Guo, M.; Hoyer, C. E.; Johansson, M.; Keller, S.; Knecht, S.; Kovačević, G.; Källman, E.; Li Manni, G.; Lundberg, M.; Ma, Y.; Mai, S.; Malhado, J. P.; Malmqvist, P. Å.; Marquetand, P.; Mewes, S. A.; Norell, J.; Olivucci, M.; Oppel, M.; Phung, Q. M.; Pierloot, K.; Plasser, F.; Reiher, M.; Sand, A. M.; Schapiro, I.; Sharma, P.; Stein, C. J.; Sørensen, L. K.; Truhlar, D. G.; Ugandi, M.; Ungur, L.; Valentini, A.; Vancoillie, S.; Veryazov, V.; Weser, O.; Wesołowski, T. A.; Widmark, P.-O.; Wouters, S.; Zech, A.; Zobel, J. P.; Lindh, R., OpenMolcas: From Source Code to Insight. J. Chem. Theory Comput. 2019, 15 (11), 5925-5964.

TOC Graphic

